

Characterisation and wear properties of industrially produced nanoscaled CrN/NbN multilayer coating

E. Bemporad^{a,*}, C. Pecchio^b, S. De Rossi^b, F. Carassiti^a

^aDept. of Mechanical and Industrial Engineering, Univ. of Rome "ROMA TRE", Italy

^bSurface Engineering Dept, Istituto Scientifico Breda S.p.A., Milano, Italy

Available online 15 September 2004

Abstract

Present work deals with morphological, microstructural, compositional and tribological characterisation of nanoscaled multilayer CrN/NbN coating produced by an industrial process presently in development phase. This coating has been applied on steel ring components used in textile plants subjected to contact erosion wear, at high frequency and low load, between the external surface of a ring and a bar where friction coefficient and corrosion resistance are critical. Nanoscaled multilayer structures usually show both high hardness and better wear resistance, correlated with grain refinement, coherency strain hardening, inhibition of dislocation motion, together with an excellent corrosion resistance due to the interruption of coating columnar pinholes and to the combined metal element effect. In order to obtain multilayer structure a non-conventional technique has been set up, consisting of triggering alternatively on Cr or Nb cathodes with appropriate time constant so as to obtain couple of layers of about 5 nm each. In order to satisfy industrial requirements, the process was optimised using a commercially available Cathodic Arc PVD equipment, routinely used to produce conventional CrN coatings.

Microstructural and compositional properties were investigated and reported hereby. Low angle X-ray diffraction, Optical and Atomic Force Microscopy, Electron Probe Microscopy (SEM, TEM, SAD, EDS) and Focussed Ion Beam techniques has been used. Defects were also investigated, particularly microdroplets (shape, dimension, density, clustering and other process-sensitive features). Mechanical and tribological properties were characterized by micro and nano hardness measurements, scratch test, ball on ring, ball-cratering and residual stresses evaluation with X-ray diffraction (XRD) $\sin^2\psi$ method. Multilayer coating shows higher H/E ratio, a clear tendency to delaminate during fracture and a different size distribution of microdroplets. As a consequence, CrN/NbN coating results in a lower wear rate with respect to the CrN coating (up to 30%) but only if a normal force dominated stress is applied. Finally, performances results (e.g. wear rate and degradation behaviour) obtained by operating in line two different sets of components (respectively CrN and CrN/NbN coated) are presented; lifetime of industrially produced multilayer coated components has been elongated from 9 to 11 months.

© 2004 Elsevier B.V. All rights reserved.

Keywords: Abrasive wheel test; PVD; Chromium; Niobium; Nitrides; Multilayer

1. Introduction

PVD coatings are suitable for improving wear resistance of components in many engineering applications. Nitride of transition metals such as CrN, TiN, NbN have been studied extensively in the past [1–4] and are presently a well-established industrial solution. Further, it is possible to

deposit such species in a periodic way so as to achieve a nanoscaled multilayer structure with improved mechanical and tribological properties as compared to single layer coatings. High coating hardness has been observed for TiN/VN [5] and TiN/NbN [6,7] multilayer coatings. Both improved corrosion resistance and decreased erosive and abrasive wear rates due to multilayer structures have also been reported for CrN/NbN [8] and TiN/CrN systems [9].

Multilayer coatings are often deposited by co-deposition in opposite targets configuration and rotating the substrate holder in order to alternately expose the substrate to the two

* Corresponding author. Tel.: +39 06 55173293; fax: +39 06 55173256.

E-mail address: e.bemporad@uniroma3.it (E. Bemporad).

targets. As the rotating substrate reaches the midway point between two adjacent targets, metal species from both targets will deposit and a mixed layer will be formed [10].

In the present investigation a non-conventional reactive cathodic arc evaporation technique is used for deposition of CrN and NbN layers by triggering alternately on Cr and Nb cathodes. Consequently, the use of interrupted deposition causes sharp interfaces between the different layers to take place without limitation of the substrate geometry.

Aim of this work is a comparison of CrN/NbN nanoscale multilayer coatings with respect to conventional CrN coatings. The study is concerned with microstructural, compositional, mechanical and tribological characterisation and includes a morphological assessment of more relevant defect present (microdroplet).

2. Experimental details

2.1. Deposition

CrN/NbN multilayer and CrN coatings were prepared in a reactive cathodic arc deposition chamber equipped with eight cathode flanges and a rotating biased carousel holding pieces for coating [11]. Films were deposited on X82WMoV65 tool steel [12] pre-polished to a roughness $R_a < 0.02 \mu\text{m}$. In the case of multilayer deposition one Cr and one Nb cathode [13] were mounted on each chamber side, in order to give a good plasma uniformity during both the CrN and the NbN layer deposition. Prior to loading into the chamber, the substrates were cleaned using a sequence of ultrasonically enhanced alkali washing stages, followed by de-ionized water rinsing and hot air drying. After loading, the chamber was pumped down to 1×10^{-3} Pa and heated for about 1 h to 350°C ; subsequently, the substrates were ion cleaned inside by an intensive bombardment with highly ionised plasma (first hydrogen and then chromium). In order to improve adhesion, a thin layer of chromium of about $0.05 \mu\text{m}$ was deposited after etching, providing a smooth transition between the ion-cleaned substrate and the coating properties. Subsequently, coatings were deposited at N_2 residual pressure of 2 Pa for CrN and 3 Pa CrN/NbN, respectively. Multilayer period is controlled during deposition by modifying the triggering time at constant deposition rate. Negative substrate Bias was set at 160 V; Cr and Nb cathode voltage was 60 and 80 A, respectively. Estimated multilayer period in the case of a 3 s triggering time, with an average deposition rate of $3 \mu\text{m}/\text{h}$ for both targets at the given target current, is about 5 nm.

2.2. Characterisation

Thickness of produced samples were measured by ball-cratering test and confirmed by cross section SEM analyses (XSEM, FEI XL30LaB₆ analytical) during inspection of coating microstructure on LN₂ fractured surfaces.

Crystallographic information was acquired by an X-ray diffraction (XRD 2θ range $30\text{--}90^\circ$ and LA-XRD, 2θ range $1\text{--}10^\circ$ using a Scintag diffractometer mod. X1 with a Bragg–Bentano geometry, 40 kV, CuK α radiation scan step: 0.01° , counting time: 4 s).

Multilayer period was measured by X-ray reflectivity (XRR) using a Bruker D8 diffractometer equipped with a Göbel mirror. The angular accuracy was 0.001° . CuK α line of a conventional X-ray source powered at 40 kV and 40 mA was used.

Homogeneity and preferential growth of coating was evaluated by cross section TEM observation (XTEM, FEI CM120LaB₆ analytical) and by FIB (FEI DualBeam). Residual stress has been evaluated using $\sin^2\psi$ method (Rigaku D-Max Rapid); the system was equipped with a cylindrical Image Plate detector able to measure two-dimensional (2D) X-ray diffraction from -45° to 160° (2θ) and a spot dimension of $300 \mu\text{m}$. Measurements were carried out at an incidence angle of 10° . The acquisition time was fixed at 60 min, the tension and current intensities were set at 30 kV and 40 mA, respectively.

Reduced Young's Modulus and absolute hardness were calculated from nanoindentation loading and unloading curve (Micromaterials NanoTest NT2, CSM NanoHardness tester, MTS Nanoindent XP); data were obtained using a Berkovich tip at various load ranging from 5 to 500 mN and elaborated using the Oliver Pharr method [14] with a Poisson's ratio of 0.3.

Micro Vickers hardness was measured by means of two independent microhardness measurements (both using Leica mod. VMHT) applying several loads between 50 and 5000 mN. The hardness was calculated by the average diagonal lengths d , measured off-line using OM and SEM. In order to extrapolate film hardness, the Chicot and Lesage and the Jonsson and Hogmark models have been used [15,16].

Coating roughness was measured both with a stylus profilometer (Taylor Hobson Talyscan 150, mechanical stylus rastering four times $1500 \times 1500 \mu\text{m}$ sample area at $2000 \mu\text{m}/\text{s}$ with $84 \mu\text{m}$ as Z range) and with an AFM (NT-MDT Smena on a $350 \mu\text{m}^2$ area in contact mode); with this latter technique also the inter-defects roughness was measured.

Defects classification was performed by optical microscopy (OM, Nikon Eclipse ME600D): images (2048×1536 pixel resolution) have been processed for isolating defects using a cascade of filters according to the following procedure: color separation (green), shading correction, sigma filter, threshold and binarize, mean ranking, morphological closing. Detected particles were classified on the basis of their dimension, sampling $1.7 \times 10^5 \mu\text{m}^2$ for each specimen [17]. The number of defects, the overall defected area and the mean shape factor have been calculated for each class, together with the mean defect number density for each type of coating.

Friction coefficient was measured with a ball on ring tribotest (Plint TE53 slim/D, ASTM G77 with sintered alumina as the counterpart).

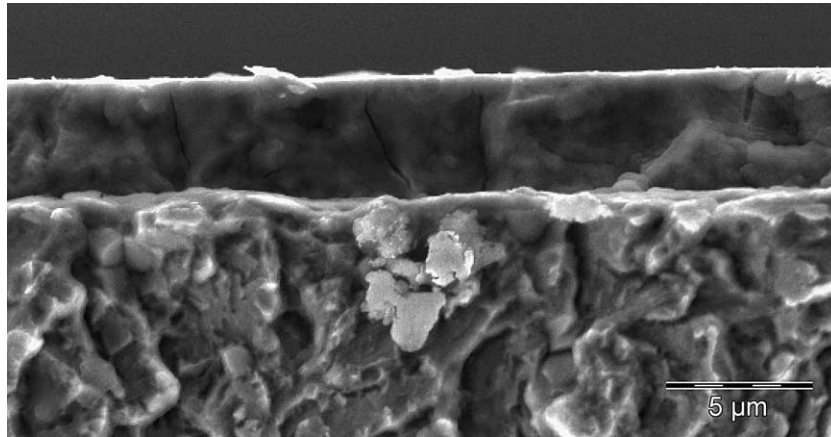


Fig. 1. LN₂ fracture surface of CrN coating; pass-through cracks are clearly visible; 15 kV, SE.

The film adhesion was measured by mean of a CSM Revetest; film adhesion and droplet adhesion were extrapolated by acoustic emission (during adhesion tests) and OM-SEM inspection of the scratched surface.

Coatings resistance to abrasive wear was evaluated with two different techniques: the Rotating Wheel Abrasive Wear Test (rotating wheel or dimple-grinder test) and the Ball Crater or Micro-Abrasion Wear Testing system (ball-cratering) using different wear loads.

The first one was performed on dimple-grinder equipment usually used to prepare TEM samples, following the procedure exposed in literature [18–22]; intrinsic abrasive wear resistance has been evaluated against a slurry of 1 μm diamond abrasives using a steel wheel of 15 mm diameter rotating at a speed of 200 rpm with a load of 0.6 N. Several test were made at different total sliding distance (for CrN coating: 47, 66, and 75 m; for CrN/NbN coating: 19, 38, and 47 m) abraded volumes were then measured with the stylus profilometer.

The second technique uses a ball-cratering calibrated for wear measurements. In this system, a steel sphere of 30 mm diameter was rotated at 100 rpm against the sample surface with the interposition of an abrading medium (1 μm diamond suspension): the sphere abraded the sample surface producing a spherical crater. While the force between the

sphere and the sample was kept constant (at 0.16 N), several measurements of the volume loss were performed varying the sliding distance.

3. Results

XSEM analyses of the LN₂ fracture surface for the two coatings are shown in Fig. 1 (CrN coating) and Fig. 2 (CrN/NbN coating). Thickness values are 3.8 μm for the CrN coating and 3.6 μm for the CrN/NbN coating.

It is also evident in observing the fracture behavior that the multilayer tends to delaminate during cracking, while CrN coating does not: cracks induced by liquid nitrogen fracture pass directly through the whole coating thickness in the case of the CrN coating and, on the contrary, move parallel to the surface in the case of the multilayer coating.

LA-XRD spectrum of the CrN/NbN coating is reported in Fig. 3. In this case, where triggering time is low enough to obtain nanometric layers, the coating shows a face centered cubic structure with a strong [200] preferred orientation. Only one peak exists between the position of CrN (NaCl-type, $a_0=0.414$ nm) and δ -NbN ($a_0=0.440$ nm). The lattice parameter calculated from [200] plane of the

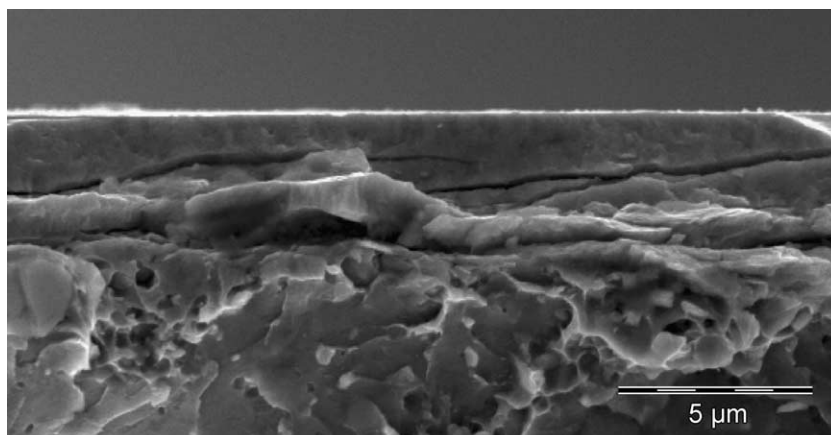


Fig. 2. LN₂ fracture surface of CrN/NbN multilayer coating; in this case cracks tend to propagate transversally; 15 kV, SE.

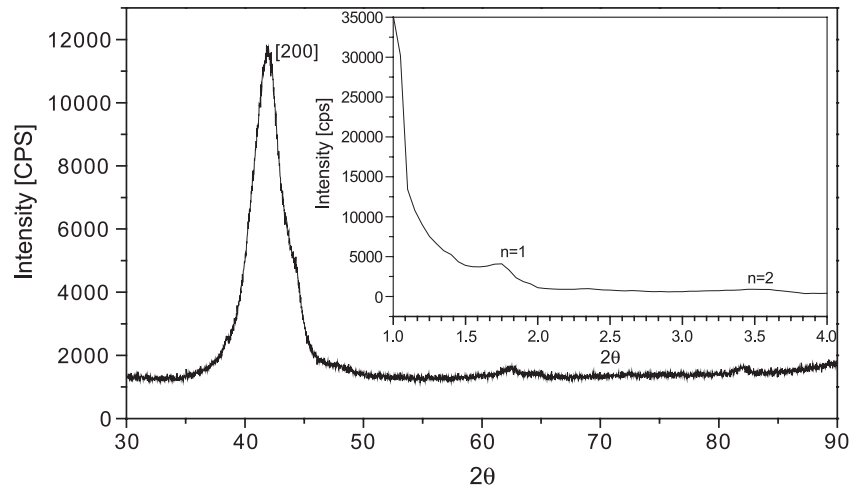


Fig. 3. High angle X-ray diffraction pattern of CrN/NbN coating. The strong [200] preferential orientation is evident. Low angle pattern (in frame), estimated multilayer period: $\lambda=5$ nm.

CrN/NbN with $\lambda=5$ nm (corresponding to $2\theta=42.14^\circ$) is 0.429 nm, indicates that CrN and NbN distort each other. The two peaks shown in the frame of Fig. 3 occurred at positions corresponding to the reciprocal lattice vector of CrN/NbN multilayer having a period λ of about 5.0 nm.

X-ray reflectivity for the same coating is reported in Fig. 4. It shows periodic peaks related with a multilayer period of 5.7 nm.

XTEM Bright Field image and top view Selected Area electron Diffraction figure of the same coating are shown in Fig. 5. Its structure results in thin layers, sharply separated each other with a clear density contrast. Electron diffraction figure confirms the [200] preferred coating orientation. The period thickness does not vary considerably and the average value, measured to be 4.7 ± 0.5 nm, is in good agreement with the value obtained by XRD measurement and with the one expected by growth conditions (triggering time and deposition rates).

FIB image of the CrN/NbN coating is shown in Fig. 6. Good homogeneity can be appreciated even for wider part of the multilayer. The thin bond layer of Cr is also visible, together with an embedded microdroplet.

Further investigation on multilayer residual stresses using $\sin^2\psi$ method is reported in Fig. 7. It was not possible to calculate the stress value due to the very broad peak at 42° ; at higher angles (about 80° with the $\text{CuK}\alpha$ X-ray source used) the intensity resulted to be too poor to carry out calculations. Nevertheless, by qualitative evaluation of the 2D spectra reported, the strong compressive state is clearly shown by the ring pattern deformation. Debye–Scherrer formula applied to the spectra reports a grain size of about 30–40 nm, very near to the multilayer period.

Hardness values obtained by the application of literature models (Chicot & Lesage model and the Jonsson and Hogmark model [13]) in order to extrapolate effective

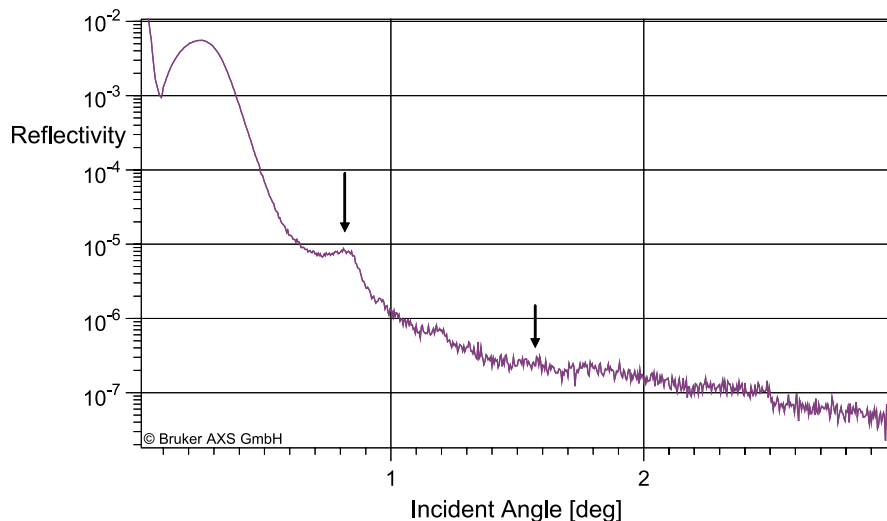


Fig. 4. X-ray reflectivity spectra; multilayer thickness is 5.7 nm, calculated with respect to the reflection indicated by the two arrows.

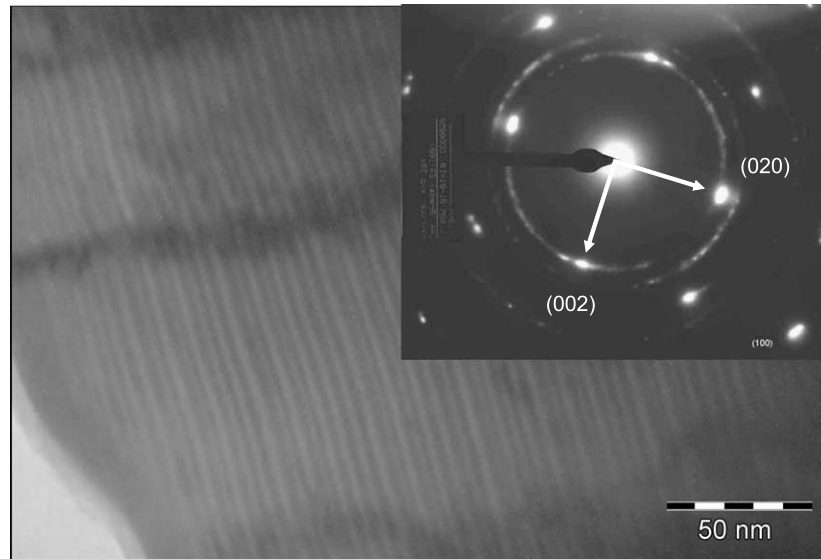


Fig. 5. Multilayer CrN/NbN period evaluation (X-TEM—120 kV, BF) and Small Aperture Diffraction Pattern (plan view).

coating hardness are reported [Table 1](#), together with a standard HV_{50} microhardness. In the case of standard HV_{50} measure, CrN/NbN coating appear to be less hard.

Models can suggest the two coatings film absolute hardness by the definition of the substrate contribution, but they are not so accurate to show difference between them.

[Table 2](#) shows Young's Modulus and absolute hardness values calculated from loading and unloading curves (an example is given in [Fig. 8](#)). Measurements were carried out directly by product specialists with three different equipment located in their respective premises. These data can be considered only from a qualitative point of view: the results are widely scattered and only measurements at a load of 20

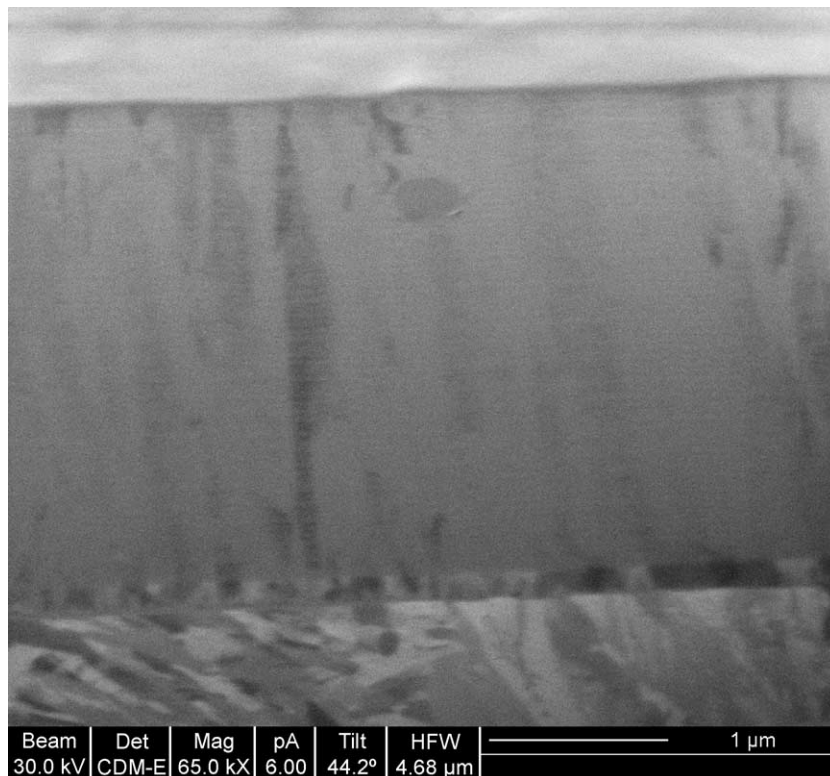


Fig. 6. Focused Ion Beam imaging of the CrN/NbN multilayered coating. A small droplet embedded into the coating is visible on the micrograph.

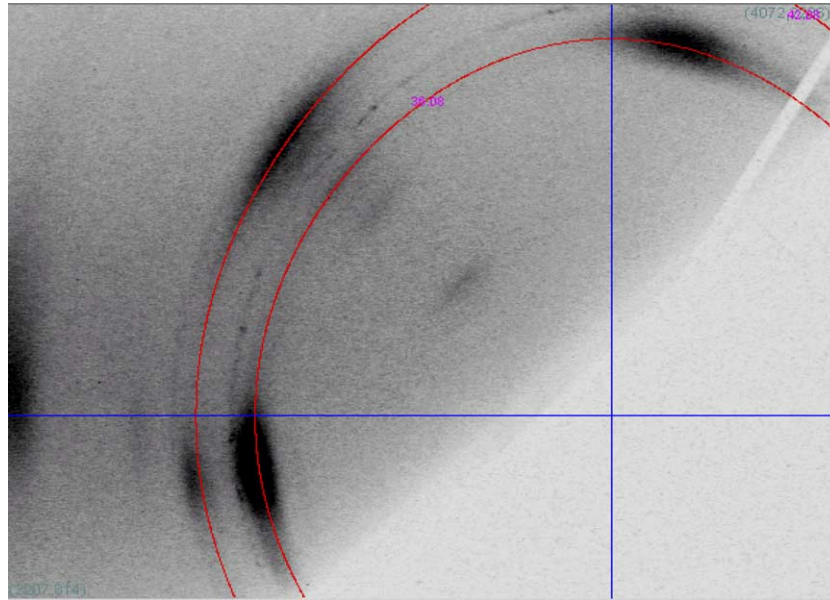


Fig. 7. 2D spectra of the CrN/NbN multilayer. It is evident the ring pattern deformation caused by a strong compressive state of the coating.

mN can be comparable. Figs. 9 and 10 show hardness and Young's Modulus obtained by Continuous Stiffness Measurement with one of the three device.

Table 3 shows roughness measurements obtained with the stylus profilometer and AFM on a quite wide area of the surface for both coatings. It is evident that CrN coating presents higher scar density on surface. Fig. 11 shows AFM scan on CrN (top) and CrN/NbN (bottom), while the overall roughness of the CrN coating surface vs. the multilayer is about twice, this ratio grows up to more than four times if only the inter-defects roughness is considered. Kurtosis value of the average roughness profile obtained with both techniques indicates that the multilayer coating defects have a wider range of dimension with respect to the monolayer one.

Figs. 12 and 13 illustrate the quantitative optical microscopy analysis of microdroplets for both coatings. In the first figure (Fig. 12) the number of microdroplets classified by projected area size is reported for each class, together with cumulative lines for both coatings. In Fig. 13, the overall defected area (that is the sum of the area of all microdroplets of a given class) is reported for each class, together with cumulative lines for both coatings.

CrN/NbN coating presents a lower number of small droplets (below $1 \mu\text{m}^2$), while there are more droplets with size of $4 \mu\text{m}^2$ and above. Multilayer CrN/NbN shows the highest value of defected area (Fig. 16): 7.42% against 5.67% of the monolayer CrN; this defected surface is mainly formed by big droplets: if only droplets up to $4 \mu\text{m}^2$ are considered, the monolayer CrN becomes more defective.

Friction coefficients, using alumina as counterpart, are reported in Fig. 14. CrN values are comparable with literature (about 0.50), while multilayer shows a value of 0.2. After about 20 m of sliding distance, multilayer coating cracks and friction coefficient rise to a contact-surface weighted value between the substrate and the film.

Wear tracks after 1200 s of sliding time are reported in Fig. 15. Images show a less amount of damage for CrN with respect of CrN/NbN coating (wider track). More flakes are also present aside from the CrN wear track.

Critical loads from scratch test are reported in Table 4, together with abrasive wear values obtained with rotating wheel and ball-cratering (abraded volumes were estimated by stylus profilometer, same equipment used to evaluate roughness). Critical load value is significantly lower for

Table 1
Standard microhardness measurement and model-extrapolated absolute surface hardness for both coatings

	CrN/NbN	CrN
Hardness HV ₅₀ , microindenter	1690	1755
Coating Hardness C&L model derived: H_0 (GPa); n	22.51; 2.05	23.84; 2.03
Coating Hardness J&H model derived: H_0 (GPa); n	23.77; 2.02	23.67; 2.04

Table 2
nanoindentation measurements (Berkovich tip, 20 mN max load)

	CrN/NbN			CrN		
	#1	#2	#3	#1	#2	#3
Reduced modulus (GPa)	246	340	460	238	291	320
Hardness (GPa)	19	28	35	17.5	22.2	24
1/(H/E)	12,95	12,14	13,14	13,6	13,1	13,33

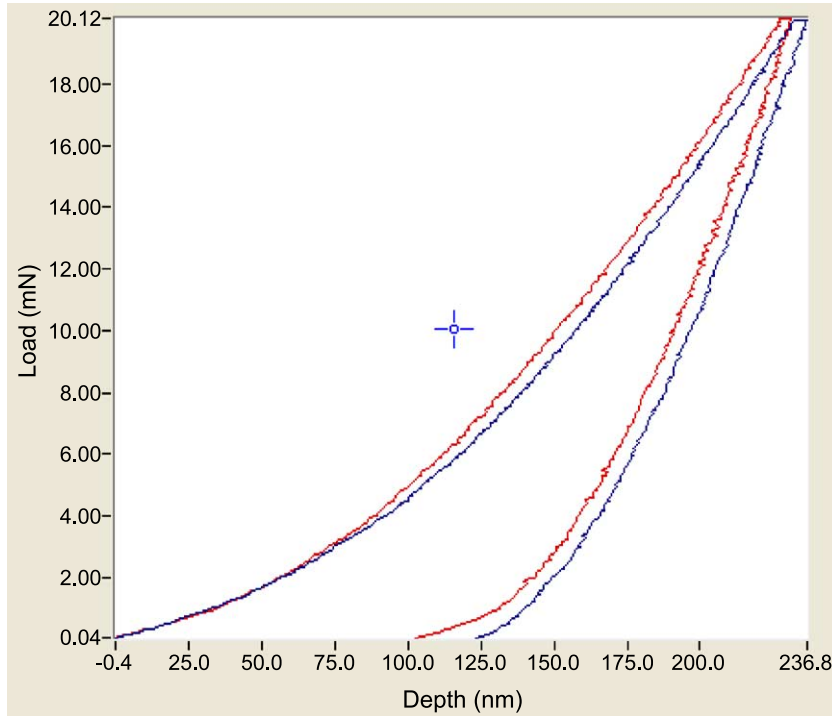


Fig. 8. Loading curve obtained with a Berkovich indenter at a max load of 20 mN; higher curve is the CrN/NbN response.

CrN/NbN multilayer coating with respect to the CrN coating. Microdroplets critical load (measured observing by SEM in the scar track first droplets removed) are the same for both coatings. Considering wear, values obtained are not in agreement for the two tests: a better performance is obtained by the multilayer coating in the case of ball-cratering while the CrN coating last longer in the case of rotating wheel test.

An example of wear craters obtained with rotating wheel and with ball-cratering are reported in Fig. 16. It can be seen

that, in the case of the rotating wheel test (upper image, left), multilayer coating tends to fail by delamination.

4. Discussion

Nanoindentation measurement can be considered only from a qualitative point of view; this can be probably related with the great difficulty to obtain reliable values for these kind of coatings with a rough surface and a lot

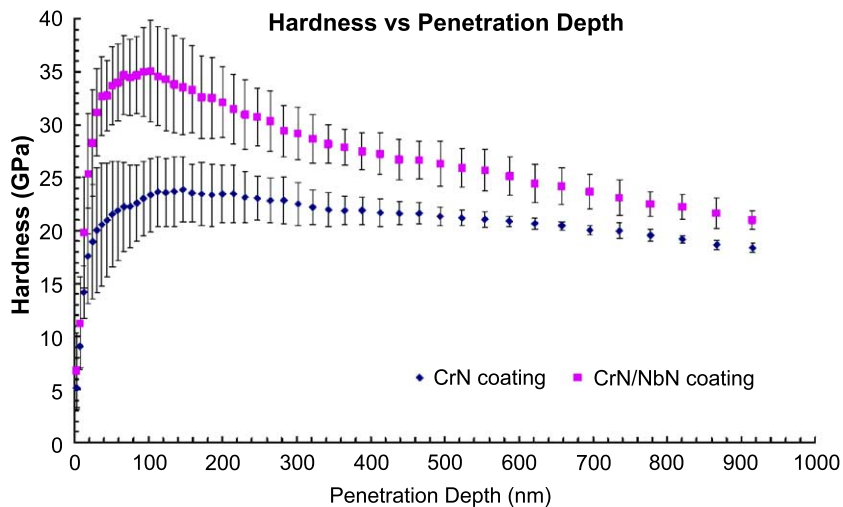


Fig. 9. Hardness vs. penetration depth obtained by nanoindentation using the Continuous Stiffness Measurement.

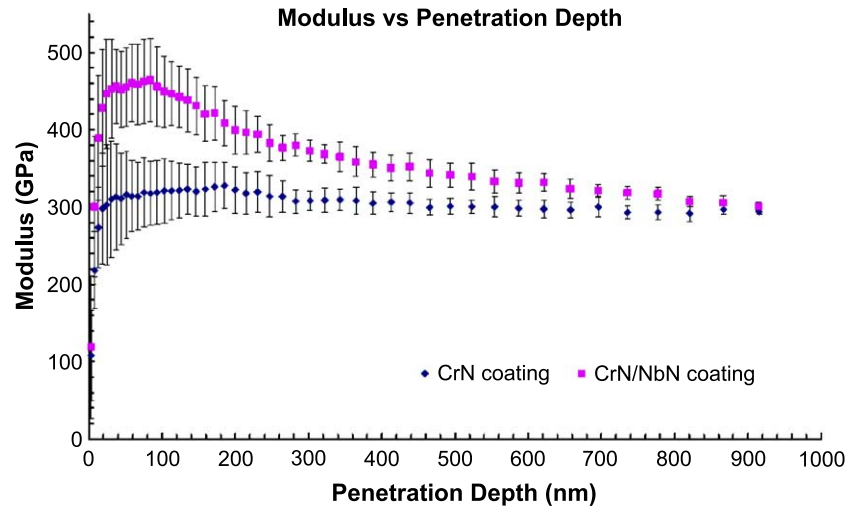


Fig. 10. Young's Modulus vs. penetration depth obtained by nanoindentation using the Continuous Stiffness Measurement.

of microdroplets (visible on the surface as well as embedded inside the film). Apart from absolute values, each equipment reported the CrN/NbN coating to be slightly harder and with a higher modulus. This difference cannot be noticed if considering only modeled hardness by micro-hardness measurements, and if only a standard HV50 measurement is performed, the multilayer coating seems to be weaker than the CrN bulk one.

Surface finishing is quite different in number and aspect of microdroplets as well as droplet-free surface. This can be correlated with the nature of the target material itself, due to the lower thermal capacity and higher melting temperature of niobium ($T_{m(Nb)}=2468\text{ }^{\circ}\text{C}$ and $T_{m(Cr)}=1890\text{ }^{\circ}\text{C}$), and the

lower temperature of cathodes that cool down during switch-off time in the frame of the alternate deposition. So the multilayer coating surface is less rough and larger droplets (that represent the highest contribution of defected surface for the multilayer coating) are easier removed from the surface during the wear test.

Nevertheless, even if multilayer film shows a higher H/E ratio, differences can be observed in failure modes: the cohesive failure of all the coatings tends to be by tensile cracking, however adhesive failure tended towards spalling for multilayer films, while chipping failure occurs along CrN wear track. Also, the behavior of scratch test shows that the multilayer does not bear shear stresses, having a lower critical load. This is more evident if ball-cratering and rotating wheel are compared: due to the difference in testing condition (different counterpart, different speed and revolution patterns, different contact surface and applied load, two or three body system during abrasion depending on slurry concentration and load) the two sets of results cannot be compared in absolute values.

It is well known, in fact, that different responses of abrasive wear testing on coatings are expected in different tribological test [23,24]. Moreover, transitions between two-body and three-body abrasive wear take place in microscale abrasive wear test depending upon test conditions [25,26]. The ball-cratering wear test is generally considered to be a three-body wear test in both "free ball" machines and "fixed ball" machines. Rotating wheel test is essentially a similar apparatus, but with different normal to shear loads ratio applied to the abraded surface. The experimental work carried out by Trezona et al. (cited above) showed that a two-body mechanism was found dominant at high loads and/or low slurry concentration; the dominant mechanism at low loads and/or high slurry concentration was a three-body process.

Table 3
Profilometer and AFM roughness measurements

Property	Symbol	Unit	Sample	
			CrN/NbN	CrN
<i>Profilometer</i>				
Surface area		μm^2	$2 \times 10^6 (\times 4)$	$2 \times 10^6 (\times 4)$
Peak to peak	Rmax	nm	390	680
Roughness	Ra	nm	30 ± 11	60 ± 17
Root-Mean-Sq	Rq	nm	54	100
Kurtosis	Rku		123	60
<i>AFM total roughness</i>				
Surface area		μm^2	200 ($\times 5$)	200 ($\times 5$)
Peak to peak	Rmax	nm	580	1450
Roughness	Ra	nm	33 ± 8	63 ± 9
Root-Mean-Sq	Rq	nm	50	115
Kurtosis	Rku		22	17
<i>AFM inter-defects roughness</i>				
Surface area		μm^2	2×15	2×15
Peak to peak	Rmax	nm	70	250
Roughness	Ra	nm	7 ± 5	30 ± 8
Root-Mean-Sq	Rq	nm	11	35
Kurtosis	Rku		3.5	3

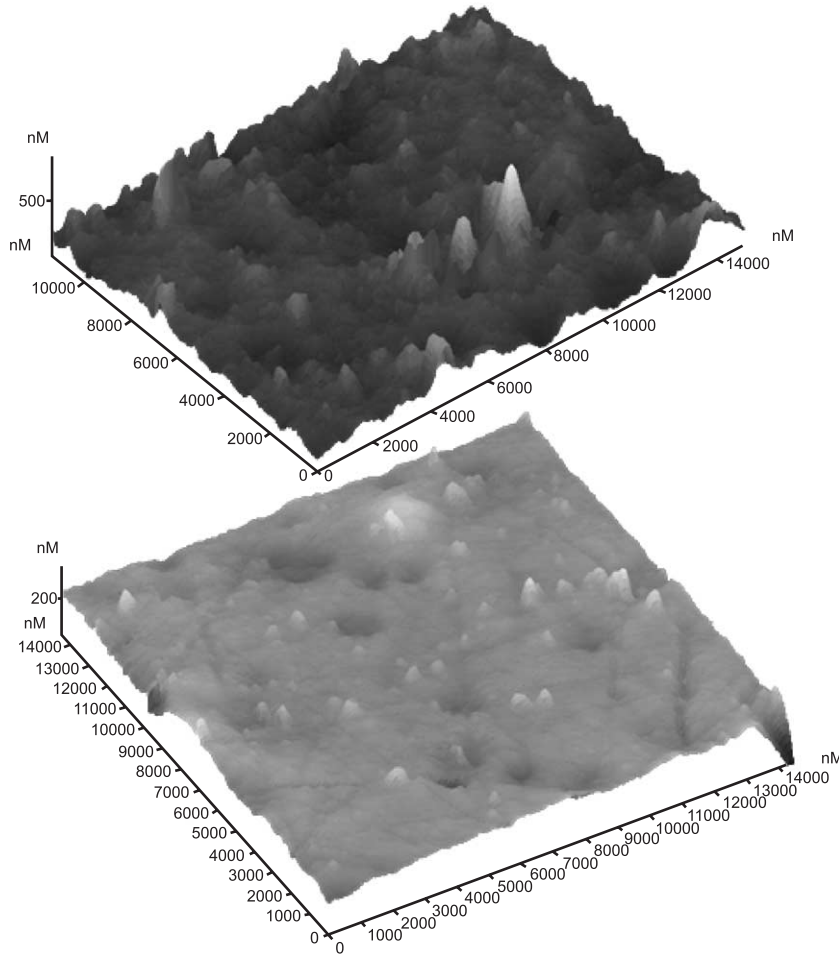


Fig. 11. 3D AFM view of CrN (upper image) and CrN/NbN (lower image) coating surfaces; scan area about 200 μm^2 .

At intermediate loads and/or slurry concentrations, some wear scars was found to display a mixed character. Micrographs of wear scars produced in this work by ball-cratering and rotating wheel display a slightly mixed

character with predominant grooving; the wear volume is found quite different unless both machines used the same type of abrasive and the same volume fraction. It is known, in fact, that wear coefficient are only directly comparable if

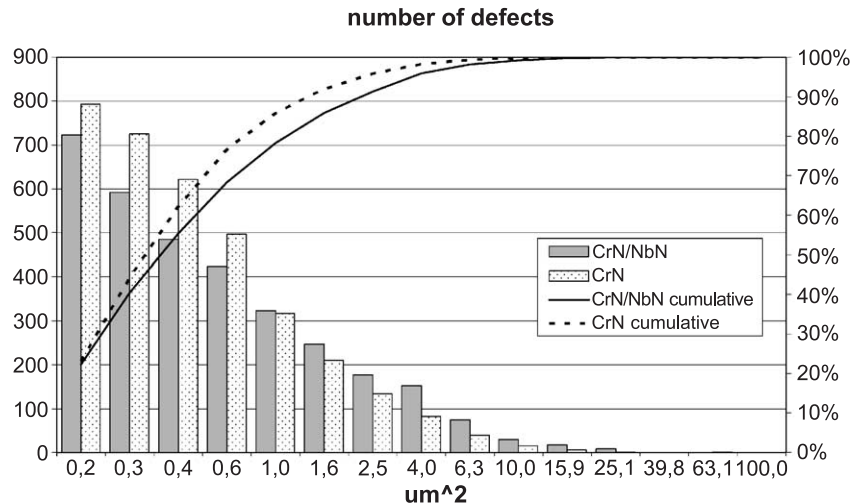


Fig. 12. Classification of defects number; multilayer coating present lower number of defects with size below 1 μm .

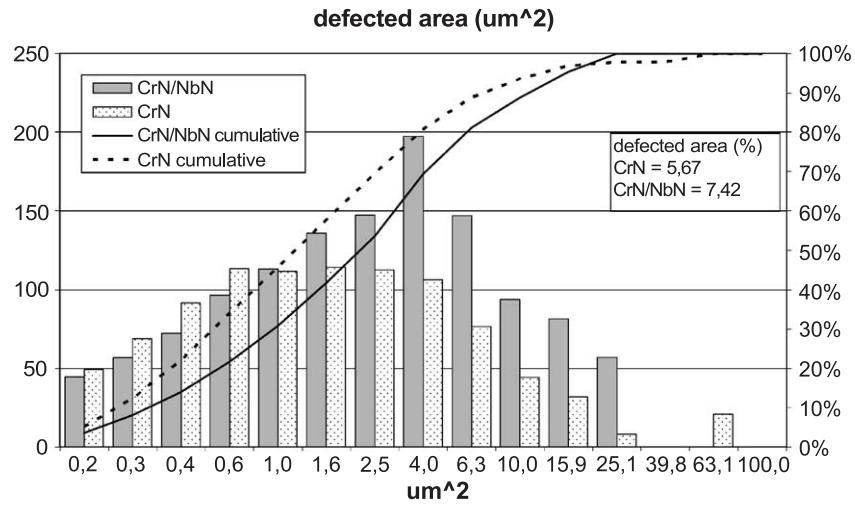


Fig. 13. Classification of defected area; multilayer coating present lower defected area if only small defects are considered.

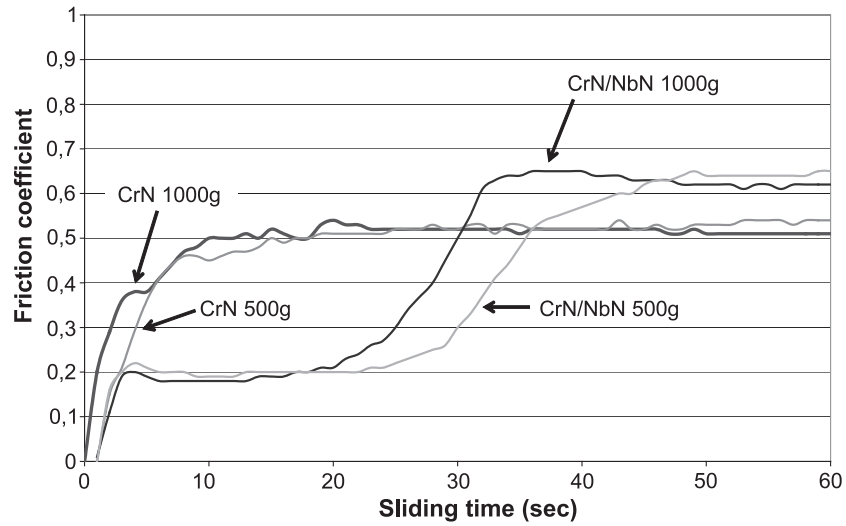


Fig. 14. Ball-on-ring wear test, friction coefficient evaluation.

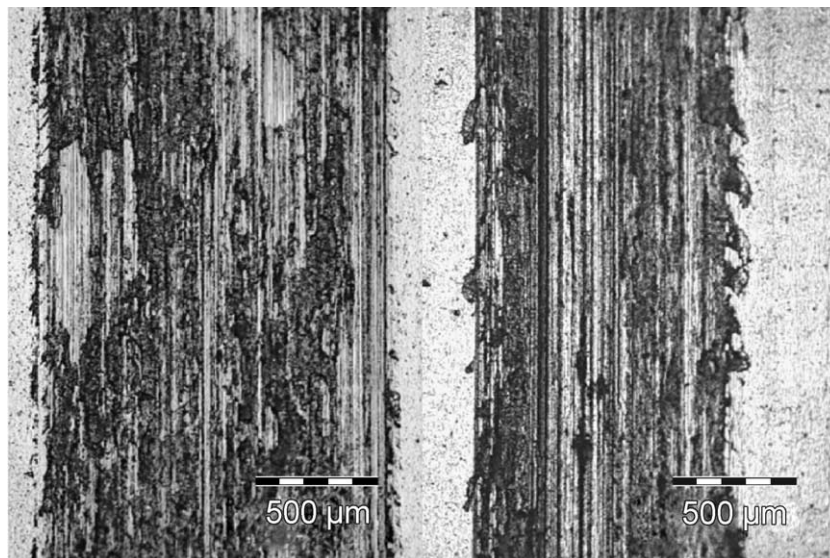


Fig. 15. Ball-on-ring wear test; wear tracks after 1200 s (10 N applied load).

Table 4
Scratch and abrasive wear test results

	CrN/NbN	CrN
Coating critical load L_c (N), scratch test	49	59
Microdroplets critical load L_c (N), scratch test	10	10
Abrasive wear of the coating Kc ($\mu\text{m}^3/\text{mm N}$), rotating wheel (with K substrate=116)	91,07	76,48
Abrasive wear Kc ($\mu\text{m}^3/\text{mm N}$), Ball-cratering	290	370

obtained under the same conditions of abrasive type and abrasive volume fraction. However, the analysis of the extension of contact area and of the values of pressure and shear in contact area shows remarkably difference between ball-cratering and dimple-grinder.

As far as CrN is concerned, the wear volume abraded in ball-cratering is higher than multiple-layer coating not surprisingly due to the lower H/E ratio. In the case of rotating wheel, instead, wear volume abraded for CrN is lower than multilayer coating because working condition with a higher shear load allows delaminating to take place, as observed in SEM and optical micrographs.

Thus, it is reasonable to think that CrN/NbN coating with a lower friction coefficient and a higher H/E ratio is able to protect the surface for a longer time during abrasion (Fig. 16

bottom left versus bottom right), except for the case of high shear stress when failure mechanisms of the multilayer coating could take place (i.e. delamination). This behavior is clearly visible in Fig. 16 (top left picture versus top right) where multilayer could be not effective in preserving the substrate from wear.

5. Conclusions

CrN/NbN nanoscale multilayer coatings with a multilayer period $\lambda \cong 5.5$ nm have been produced by cathode switching reactive cathodic arc evaporation. The deposition of multilayers was carried out using interrupted deposition by alternately triggering on two cathodes (Cr, Nb) in order to obtain sharp interfaces. X-ray diffraction and TEM analysis confirmed the formation of a homogeneous and compact multilayer structure demonstrating that the method of alternately triggering cathodes is an effective process to obtain desired structured coating with designed period. Typical defects (droplets) are reduced because of lower thermal capacity and higher melting temperature of Nb. Also, multilayer coatings resulted to be less coarse than bulk ones, especially if surface not affected by droplets is considered. Mechanical and tribological properties have been compared with a standard CrN coating produced in the same deposition equipment. A different preferential behav-

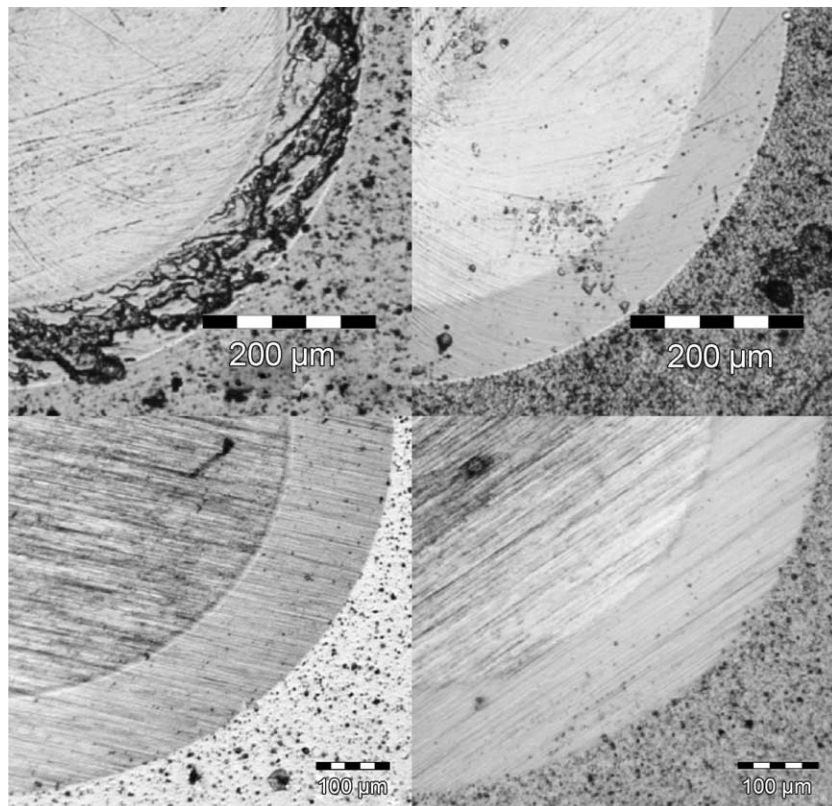


Fig. 16. Wear track obtained with the Rotating Wheel (RA) and Ball-cratering (BC); from top to bottom, left to right: CrN/NbN (RA); CrN (RA); CrN/NbN (BC); CrN (BC).

ior of coating failure has been observed, tensile cracking for CrN coating and delamination for multilayer coating. Multilayer CrN/NbN coating, due to higher hardness vs. Young's modulus ratio, and lower friction coefficient are candidate to protect surfaces for a longer time against abrasion, while when failure mechanisms of the multilayer coating could take place, i.e. delamination, multilayer could be not as effective in preserving the substrate from wear. A successful industrial application of this type of coating can be reported on a steel ring components used in textile plants. This application is characterized by a contact, at a high frequency and low load, between the external surface of a ring and a bar. CrN/NbN coating, deposited on the ring, improves the components performances of about 30% with respect to CrN coating. In this case, lifetime has been improved from 9 up to 11 months.

Acknowledgments

Morphological and compositional analysis have been carried out at the "Interdepartmental Laboratory of Electron Microscopy" (LIME), University of Rome "ROMA TRE" (<http://www.lime.uniroma3.it>) with the cooperation of Daniele De Felicis. Authors would like to acknowledge Elza Bontempi and Marcello Gelfi from the General and Structural Chemistry Laboratory, Department Mechanics, University of Brescia; for residual stress measurements, Gregory Favaro, CSM Instruments, Peseux, SWITZERLAND, Ben Beake, Micro Materials, Wrexham, UK, and Michel Fajfrowski, MTS Systems, F for nanoindentation measurements. Thanks also to Francesco Tatti, FEI analytical Italia, for collaborating during FIB analyses and Alessio Loreto, University of Rome La Sapienza dip. ICMMPM Materials Science and Technology Lab. for surface measurements with the stylus profilometer.

References

- [1] G. Berg, C. Fredrich, E. Broszeit, C. Berger, *Surface and Coatings Technology* 86/87 (1996) 184.
- [2] C. Gautier, J. Machet, *Thin Solid Films* 295 (1997) 43.
- [3] H.A. Jehn, J.-H. Kim, S. Hofmann, *Surface and Coatings Technology* 38 (1988) 715.
- [4] W.D. Sproul, P.J. Rudnik, M.E. Graham, *Surface and Coatings Technology* 39/40 (1989) 355.
- [5] U. Helmersson, S. Todorova, S.A. Barnett, J.-E. Sundgren, L.C. Mrkert, J.E. Greene, *Journal of Applied Physics* 62 (1987) 481.
- [6] X. Chu, M.S. Wong, W.D. Sproul, S.L. Rohde, S.A. Barnett, *Journal of Vacuum Science and Technology A* 10 (4) (1992) 1604.
- [7] M. Larsson, P. Hollman, P. Hedenqvist, S. Hogmark, U. Wahlstrom, L. Hultman, *Surface and Coatings Technology* 86/87 (1996) 351.
- [8] M. Tomlinson, S.B. Lyon, P. Hovsepian, W.D. Munz, *Vacuum* 53 (1999) 117.
- [9] M. Nordin, M. Herranen, S. Hogmark, *Thin Solid Films* 348 (1999) 202.
- [10] D.C. Cameron, R. Aimo, Z.H. Wang, K.A. Pischow, *Surface and Coatings Technology* 142/144 (2001) 567.
- [11] Multi-arc 3344, Multi-Arc Inc. International, 1990 Christensen Av., St. Paul, MN 55118, US.
- [12] S600 (Böhler designation), hardened and tempered at 550 °C (Young Modulus=217 GPa).
- [13] E. Bemporad, C. Pecchio, L. Martinelli, S. De Rossi, F. Carassiti, *Proceedings of the ICAMM 2003 Durban, South Africa*, ISBN: 1-86840-501-X, 2003 (January) p. 290.
- [14] W.C. Oliver, G.M. Pharr, *Journal of Materials Science* 7 (1992) 1564.
- [15] O. Vingsbo, S. Hogmark, B. Jönsson, A. Ingemarson, in: P.J. Blau, B.R. Lawn (Eds.), *Materials Science and Engineering*, 1986, p. 257, ASTM STP 889.
- [16] D. Chicot, J. Lesage, *Thin Solid Films* 245 (1995) 123.
- [17] C. Pecchio, E. Bemporad, D. De Felicis, S. De Rossi, F. Carassiti, *7 Surface Treatments VI*, WIT press, 2003, p. 61.
- [18] R. Gahlin, M. Larsson, P. Hedenqvist, S. Jacobson, S. Hogmark, *Surface and Coatings Technology* 90 (1997) 107.
- [19] K.L. Rutherford, S.J. Bull, E.D. Doyle, I.M. Hutchings, *Surface and Coatings Technology* 80 (1996) 176.
- [20] K.L. Rutherford, I.M. Hutchings, *Surface and Coatings Technology* 79 (1996) 231.
- [21] M. Berger, U. Wiklund, M. Eriksson, H. Engqvist, S. Jacobson, *Surface and Coatings Technology* 116–119 (1999) 1138.
- [22] E. Martinez, U. Wiklund, J. Esteve, F. Montalà, L.L. Carreras, *Wear* 9237 (2002) 1.
- [23] J.C.A. Batista, C. Godoy, G. Pintaude, A. Sinatora, *Surface and Coatings Technology* 174–175 (2003) 891.
- [24] Xiaodong Zhu, W. Lauwerens, P. Cosemans, M. Van Stappen, J.P. Celis, L.M. Stals, Jiawen He, *Surface and Coatings Technology* 163–164 (2003) 422.
- [25] R.I. Trezona, D.N. Allsopp, I.M. Hutchings, *Wear* 225–229 (1999) 205.
- [26] K. Adachi, I.M. Hutchings, *Wear* 255 (2003) 23.